Theor Chem Acc (2001) 106:105–112
DOI 10.1007/s002140000247

Theoretical
Chemistry Accounts

Regular article

Quantum mechanical/molecular mechanical methods and the study of kinetic isotope effects: modelling the covalent junction region and application to the enzyme xylose isomerase

R. Mark Nicoll, Sally A. Hindle, Grant MacKenzie, Ian H. Hillier, Neil A. Burton

Department of Chemistry, University of Manchester, Manchester M13 9PL, UK

Received: 19 July 2000 / Accepted: 6 September 2000 / Published online: 21 March 2001

Abstract. Hybrid quantum mechanical and molecular mechanical (QM/MM) methods are used to estimate the kinetic isotope effects (KIEs) for the 1,2 hydride shift reaction of xylose isomerase. Semiclassical transition-state theory with multidimensional tunnelling corrections are evaluated with both semiempirical and ab initio density functional hybrid methods for the study of enzyme catalysis. As part of the study, a link atom and a modified localised self-consistent-field method are assessed to represent the QM and MM covalent interface region. We have shown for some model systems that although the bond orbital method can be adjusted to perform better than the link atom method by using auxiliary density basis functions or by charge scaling, in general the link atom method performs as well. Several QM/MM models are used to calculate the xylose isomerase potential-energy surface and the importance of tunnelling for the KIEs beyond the Wigner correction is demonstrated.

Key words: Xylose isomerase – Quantum mechanical/molecular mechanical methods – Localised self-consistent field – Enzyme catalysis – Kinetic isotope effect

1 Introduction

Xylose isomerase (EC 5.3.1.5) is a much-studied enzyme which catalyses the interconversion of the isomeric forms of a range of sugars [1]. Found in a number of microorganisms, xylose isomerase is particularly important industrially in the production of high-fructose corn syrup, which can be used as a sweetener in preference to sucrose. In this study we have investigated the mechanism of the reversible conversion of the aldose D-xylose isomer (**I**) into the ketose D-xylulose isomer (**II**) using hybrid quantum mechanical and molecular mechanical (QM/MM) computational techniques.

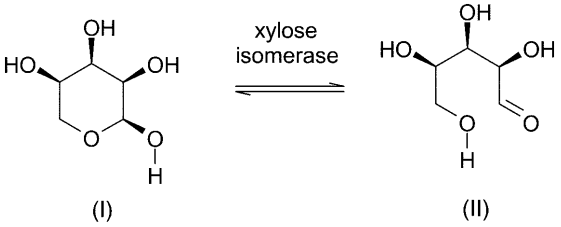

(I) (II)

The mechanism of xylose isomerase has been previously investigated both experimentally [2–7] and computationally [8–11] and the rate-limiting step is generally agreed to involve a 1,2 hydride shift. There is a great deal of discussion at present regarding enzymatic hydrogen-shift mechanisms and the interpretation of the associated experimental kinetic isotope effects (KIEs), in particular the role of quantum mechanical tunnelling. In this article we discuss the use of QM/MM methods to study the KIEs of the xylose isomerase hydride shift step.

Hybrid QM/MM methods [12–14] are becoming particularly useful for the study of enzymatic mechanisms since they allow the important aspects of reactivity involving electronic rearrangements to be studied quantum mechanically, whilst the remainder of the enzyme system is approximated at a lower theoretical level, here using molecular mechanics. These methods have been reviewed recently [15].

In this study we discuss an ab initio QM/MM implementation which utilises the Hartree–Fock (HF) and density functional theory methods, which should be more reliable than the more widely used semiempirical methods. One of the major problems faced in the development of new techniques for the study of condensed-phase systems such as enzymes is to gauge their applicability and accuracy. High-level ab initio methods have now been shown to be extremely reliable for gas-phase studies of small molecules and it is now possible to favourably compare computationally determined kinetic parameters, such as KIEs or rate constants, with those from experiment [16, 17]. Here, we extend these

Correspondence to: N. A. Burton

Contribution to the Symposium Proceedings of Computational Biophysics 2000

techniques, involving semiclassical variational transition-state theory (VTST), towards the study of the kinetics of enzyme catalysis using QM/MM methods.

In these QM/MM methods the molecular system will be divided into two distinct regions, one of which will be treated quantum mechanically, the other will be treated classically (MM). The MM region is allowed to interact with the QM region as a perturbation to the QM Hamiltonian with the electrostatic and steric effects readily introduced through the interaction with a standard MM force field. In this work we include the electrostatic potential of the partial charges as a one-electron perturbation and the other effects, van der Waals, bond, angle and dihedral interactions between QM and MM regions, are introduced additively [18–20] using the AMBER force field [21].

An important aspect in the development of accurate techniques for the study of condensed-phase reactivity is this interaction between the QM and MM regions. For many enzyme systems it is inappropriate to separate the system into a QM and a MM region without partitioning across a covalent bond. There are two main approaches for approximating this junction between the two regions: the link atom method, whereby covalent bonds are approximated by real bonds to hydrogen atoms (Fig. 1a), and (localised) bond orbital methods [22–27], where an approximate localised orbital is added to the quantum region (Fig. 1b). In both of these approaches it is necessary that the valency in the QM region is fully satisfied. The link atom method [14] is probably the most commonly applied scheme although the bond orbital methods may now be more appropriate to improve the accuracy offered by ab initio QM/MM methods. Here, we compare two schemes, a link atom method and the localised self-consistent-field (LSCF) method [22] and discuss how they may be adjusted for increased applicability. The schemes are applied to study the energetics of the xylose isomerase reaction.

2 Representation of the QM/MM interface region

In this section we discuss two approaches for the description of the QM/MM interface when the QM and MM regions are partitioned across a covalent bond. In the discussion to follow we refer to the QM and MM atoms which form part of this covalent bond as the (QM-) bond atom and the (MM-) junction atom, respectively (Fig. 1).

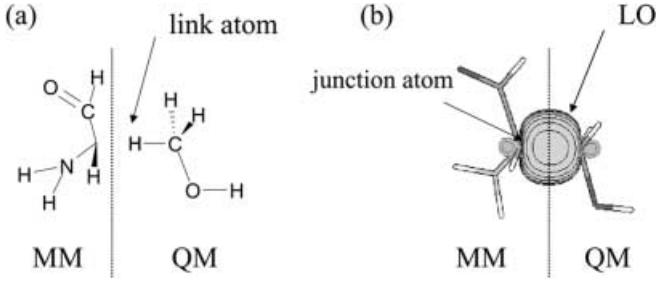

Fig. 1. The quantum mechanical/molecular mechanical (*QM/MM*) interface region using **a** a link atom and **b** the localised self-consistent-field (*LSCF*) method with a localised bond orbital

The first and most common approach is to use a link atom, introduced into the QM region to terminate any dangling bonds at the bond atoms. In our link atom scheme we introduce a hydrogen (link) atom, 1.0 Å from the quantum bond atom. The junction atom now forms part of the MM region and should, therefore, have a partial charge associated with it; however, since this charge would be too close to the new QM hydrogen link atom, it is usually set to zero and to maintain the original (neutral or integral anionic/cationic) charge of the overall system, any excess charge is divided equally amongst the MM atoms adjacent to the junction atom. This method has been applied quite successfully to proteins [18–20] by partitioning between C_α and C_β atoms since the C_α charge is often near zero and, thus, there is minimal perturbation. Furthermore, the size of the quantum region is generally chosen to be large to avoid adverse termination effects.

An alternative scheme to describe the interface region in ab initio QM/MM methods is the LSCF method originally proposed by Assfeld and Rivail [22]. In this method the dangling bonds are retained in the QM calculation as localised bond orbitals (LOs). Central to this scheme is the reorthogonalisation of the atomic orbital basis to the localised orbitals by way of a transformation matrix, $\mathbf{B}$[1]. This ensures that the final molecular orbitals from the QM calculation are orthogonal to the junction bonds and that the overall valency of the system is maintained.

Following the nomenclature of Assfeld and Rivail, the SCF procedure of an ab initio HF or Kohn–Sham (KS) density functional program can be modified through an initial transformation of the Fock (or KS matrix).

$$\mathbf{F}' = \mathbf{B}^{+} \cdot \mathbf{F}^{\mathrm{AO}} \cdot \mathbf{B} \ ,$$

where $\mathbf{B} = \mathbf{M}^{+}.\mathbf{X}$ and

$$\mathbf{M}_{\mu\nu} = \left(1 - \sum_{i}^{L} \mathbf{S}_{\mu i}^{2}\right)^{-\frac{1}{2}} \left(\delta_{\mu\nu} - \sum_{i}^{L}\sum_{\eta}^{N} a_{\nu i} a_{\eta i} \mathbf{S}_{\eta\nu}\right) \ .$$

The coefficients, a, are those of the L orthogonalised localised orbitals and $\mathbf{S}$ is the usual overlap matrix over N basis functions.

There are a number of issues associated with the use of the LSCF method. The main issue is that the localised orbital can be associated with two electrons, and thus an additional negative charge is effectively included in the quantum calculation for each LO present. To balance this electron from the junction atom, a charge (q_{add}) of $1.0e$ is added to the original junction atom partial charge. We have found that the value of this charge can become quite problematic, especially for more ionic systems, and we propose a modified scheme later to improve the performance. We have also found that convergence of the SCF procedure required a redefinition

[1] We note that we use a transformation matrix $\mathbf{B} = \mathbf{M}^{+}.\mathbf{X}$ here and not $\mathbf{B} = \mathbf{M}.\mathbf{X}$ as stated in Ref. [22].

of the DIIS error matrix, error = **F′P′**–**P′F′**, where the prime indicates the reduced dimension transformed (orthogonal) basis resulting from orthogonalisation to the LOs. The LOs were constructed from model calculations using the Boys localisation procedure and all MO coefficients not corresponding to the bond or junction atoms were set to zero.

The link atom and LSCF schemes were implemented into a modified version of GAUSSIAN94 [28] and our QM/MM interface to AMBER4.1 [29].

2.1 Comparison of link atom and LSCF schemes

In order to gauge some of the relative merits of the two QM/MM interface schemes in a QM/MM environment, we studied the proton affinities and geometries of molecules (Fig. 2) modelling the serine (Ser) and histidine (His) amino acids.

In each case the model system (neutral Ser and protonated His) was fully optimised at the HF level using a 6-31G* basis set. This geometry was subsequently used for all further tests with the QM/MM methods where the amino acid backbone (CHO.CH.NH_2) was fixed and treated at the MM level with the AMBER force field, which was modified by re-evaluation of the electrostatic potential fitted charges [30] for the model system. In all cases the electrostatic potential charges from the neutral molecule were used. The QM/MM calculations were also performed at the HF/6-31G* level for consistency.

The localised C_α-C_β orbitals for the LSCF method were obtained using the Boys localisation scheme. Table 1 shows the proton affinity differences for the two reactions relative to the proton affinities calculated at the full HF/6-31G* level (Fig. 2).

The quantum regions (amino acid side groups) of the two neutral model systems were then optimised using the two QM/MM methods with the bond (and therefore

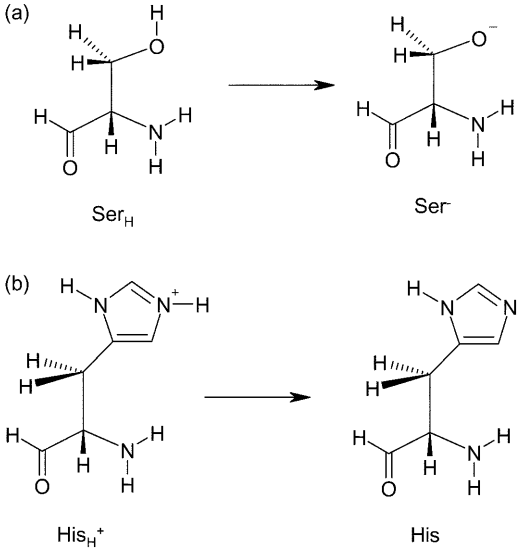

Fig. 2. Schematic structures for **a** the $Ser_H \rightarrow Ser^-$ and **b** the $His_H{}^+ \rightarrow$His model reactions

Table 1. Proton affinity differences (kcalmol^{-1}) of the quantum mechanical/molecular mechanical (*QM/MM*) method relative to the all-electron Hartree–Fock(*HF*)/6-31G* method for $Ser_H \rightarrow Ser^-$ and $His_H^+ \rightarrow$His

	Ser	His
Localised self-consistent field $q_{add} = 1.0$	−2.35	−6.59
Link atom	11.9	−5.03

Table 2. Geometry differences per atom (Å) for the QM/MM method relative to the all-electron HF/6-31G* method for Ser_H and His models

	Ser	His
Link atom	0.32	0.33
Localised self-consistent field $q_{add} = 1.0$	0.64	1.31
Localised self-consistent field $q_{opt\text{-}g}$	0.30	0.38

link) atoms fixed during optimisation [31]. The absolute mean deviations per atom between the full all-electron HF/6-31G* method and the QM/MM optimised structures are presented in Table 2.

In comparison with the full ab initio results, the link atom QM/MM method is seen to perform well compared to the rather more elaborate LSCF method. This trend is also observed for the geometries of other amino acid models [32], which we have not presented here since the Ser and His cases show the greatest deviations.

2.2 Adjustment of the QM/MM schemes

In order to achieve an improved performance of the QM/MM schemes we consider possible optimisation of the bond representations. Since there is no unique definition of localisation, there are necessarily a range of possible schemes for obtaining the localised orbitals including direct optimisation of the orbital coefficients (or pseudopotential parameters [27]) for a particular property of the model system. Such a procedure can become quite laborious, especially for each new system to be studied, and so in this study we chose to use orbitals localised using conventional localisation schemes. In our preliminary geometry optimisation studies we found little difference between, for example, Boys [33] and Pipek–Mezey [34] localisation schemes, and little advantage to using simple generic orbitals, such as those from C_2H_6, despite the associated conformational problems.

We consider two simple alternative schemes to tune the junction regions:

1. Adjusting the junction atom charge from q_{add} to q_{opt}.
2. Delocalisation of the junction atom charge.

In the first LSCF scheme, the charge (q_{add}) added to the junction atom is usually 1.0*e*. By optimisation of this partial charge (q_{opt}) the performance of the LSCF method may be improved; however, as with the link

atom method, where this charge is set to zero, we must ensure that the charge of the overall system is retained (i.e. neutral, ionic or cationic). This was achieved by spreading the excess charge ($1.0 - q_{opt}$) evenly over the MM atoms adjacent to the junction atom. One potential criticism of such a charge adjustment scheme is that the overall charge distribution in the interface region can become unrealistic. To avoid this we consider an alternative scheme proposed for link atoms by Brooks [35], whereby the junction atom charge can be simply "blurred" using an auxiliary "density" basis function (DBF). Here the point charge, $q = 1.0 + q_{mm}$, is replaced by a Gaussian distribution, $q\exp(-\alpha_{DBF}[R_J - r]^2)$, whose exponent, α_{DBF}, can be varied to delocalise the charge density and attenuate problems associated with the proximity of this charge and the QM wavefunction. The absolute proton affinities for the two model systems of the QM/MM LSCF method can be improved by optimisation of the junction atom point charge (LSCF q_{add}, Fig. 3a) and the junction atom exponent (LSCF/DBF, Fig. 3b) of the DBF. In both cases we note that the full ab initio proton affinity differences could be reproduced exactly. However the results shown in Table 3 correspond to values of 0.97 and 30.0 for Ser and 0.45 and 0.08 for His for q_{opt} and α_{DBF}, respectively, where the original junction atom partial charges (q_{mm}) for Ser and His were large, 0.41 and 0.53, respectively. In each case significant improvement of the accuracy of the QM/MM method was achieved over the original link atom method.

In a QM/MM LSCF scheme analogous to that discussed earlier, we optimised a junction atom charge, $q_{opt\text{-}g}$, to minimise the absolute mean difference per atom between the fully ab initio and the LSCF coordinates. Here the LSCF orbital remained invariant and stationary throughout the optimisation, allowing us to make only minimal code changes to utilise analytic gradients for the LSCF method. In this case (Table 2, $q_{opt\text{-}g} = 0.8$ and 0.6 for Ser and His, respectively) we were not able to exactly reproduce ab initio optimised geometries, but the LSCF method was able to consistently match the accuracy of the link atom method. However it is important to remember that the MM force field was not optimised for this study and it will play an important role in determining the QM/MM geometries.

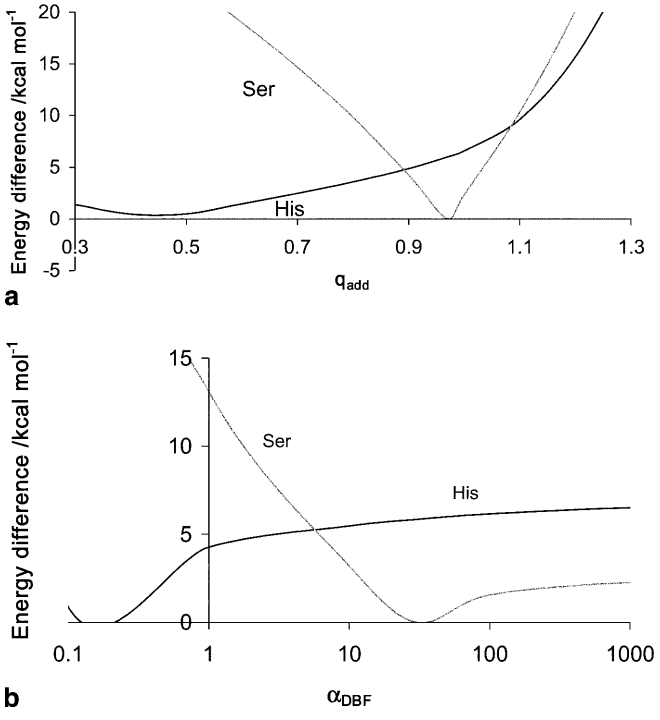

Fig. 3. Absolute proton affinity differences of the QM/MM LSCF method relative to the full Hartree–Fock/6-31G* method versus **a** q_{add} and **b** α_{DBF}

Table 3. Proton affinity differences ($kcalmol^{-1}$) from optimised QM/MM methods relative to the HF/6-31G* method for $Ser_H \rightarrow Ser^-$ and $His_H^+ \rightarrow His$

	Ser	His
Localised self-consistent field q_{opt}	−0.25	−0.01
Localised self-consistent field/density basis function $q_{add} = 1.0$	0.02	0.18

3 Application of the QM/MM method to the isomerisation reaction of xylose isomerase

The first step of the catalytic reaction of xylose isomerase is ring opening to allow the sugar to form the enzyme–substrate complex. This is followed by the rate-limiting isomerisation step, involving a 1,2 hydride shift, shown in Fig. 4. The active site of xylose isomerase contains two magnesium atoms, which are essential for the activity of the enzyme. One of these magnesium ions, $Mg_{(1)}$, is believed to assist the binding and opening of the sugar ring and the other, $Mg_{(2)}$, has been located in two different positions using X-ray crystallographic techniques and we shall consider its position carefully. In the following sections we use QM/MM methods to study the kinetics of the hydride shift reaction in the enzyme.

3.1 QM/MM active site models

Our hybrid QM/MM models are based upon two crystallographic structures of the enzyme, 6XIM [4] and 4XIS [6] arising from actinoplanes missouriensis and streptomyces rubiginosus. With D-xylose as the substrate, hydrogen atoms were added to the enzyme structures, which were then solvated within AMBER 4.1 followed by geometry optimisation at the MM level. Dimeric structures were used in subsequent calculations since the active site is made up from residues of each monomer unit and the optimised monomer did not

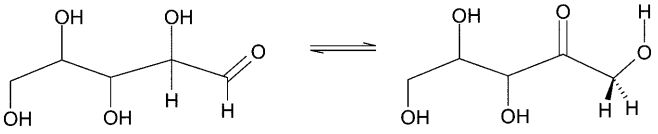

Fig. 4. The 1,2 hydride shift reaction in xylose isomerase

deviate significantly from the structure of the experimental dimer/tetramer. Since molecular dynamics simulations showed the enzyme to be quite rigid, the energy-minimised initial structures for the MM region were used in all QM/MM calculations.

3.2 Effects of the QM/MM interface region

It is useful to extend our model studies described earlier and to consider the effect of the QM/MM interface region on the energetics and mechanism of this enzymic reaction. In this section we compare the link atom method with that of the LSCF method for the xylose isomerase hydride shift reaction. Using a QM/MM model derived from the 4XIS crystal structure we considered a small six-residue QM region as illustrated in Fig. 5, which includes the xylose substrate, Glu-216, Leu-182 and His-53, a water molecule and the two Mg^{2+} ions.

The active site (QM) residues were each partitioned between the C_α-C_β bonds, with the side-chain atoms treated quantum mechanically and free to optimise. Stationary points for the reactant, product and transition state were located using QM/MM methods and activation barriers for the forward and reverse reactions were computed. The HF method and a small 3-21G basis set was used with the three interface regions of Glu, Leu and His treated using the link atom method, using the LSCF method with $q = 1.0$ and using the LSCF method with $q_{\text{opt-g}}$ parameterised with the geometry minimisation scheme outlined in the previous section. The $q_{\text{opt-g}}$ charges were 0.8, 0.8 and 0.6 for Glu, Lys and His, respectively. The resulting activation barriers are presented in Table 4 and we can see the same trend as

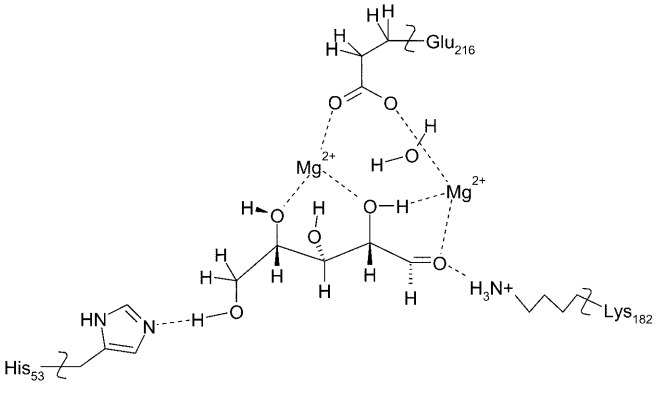

Fig. 5. The six-residue QM/MM model active site

Table 4. A comparison of forward ($\Delta E_{\text{forward}}$) and backward ($\Delta E_{\text{back}}$) activation barriers (kcalmol^{-1}) for the xylose isomerase hydride shift using link atom and localised self-consistent-field QM/MM methods at the HF/3-21G level

QM/MM method	$\Delta E_{\text{forward}}$	ΔE_{back}
Link atom	40.8	24.6
Localised self-consistent field $q_{\text{add}} = 1.0$	37.9	31.8
Localised self-consistent field q_{opt}	39.8	26.9

observed with the amino acid studies; The values predicted by the LSCF method and the link atom methods do not differ substantially from each other and the adjustment of the LSCF charge to q_{opt} brought greater agreement, although its effect for the reverse barrier is somewhat larger.

From these results we would not expect termination effects to be significant in this system and use the simpler link atom approach in further studies. In each case the barriers predicted here, about 40 kcalmol^{-1}, are quite large and the discrepency with experimental values, nearer 14–18 kcalmol^{-1} [2, 3], clearly lies elsewhere.

3.3 Alternative QM/MM models for the isomerisation step

We now consider an alternative model of xylose isomerase derived from the more recent 6XIM crystal structure in order to compare with experimental KIEs. Here we studied the potential-energy profile from a range of QM methods, in each case optimising bound reactant and product geometries and finding transition states corresponding to the 1,2 hydride shift. In each case the QM region included the xylose substrate, Glu-216 and the two magnesium ions. One magnesium ion, $Mg_{(1)}^{2+}$, was bound in its crystallographic position. For the second ion, $Mg_{(2)}^{2+}$, there are two alternative positions suggested from X-ray studies for the 4XIS structure, denoted $Mg_{(2a)}^{2+}$ and $Mg_{(2b)}^{2+}$ in Fig. 6; however, for the 6XIM structure only the $Mg_{(2a)}^{2+}$ position, closer to the substrate is observed.

We compare the forward activation barrier for this reaction with the two alternative $Mg_{(2a)}^{2+}$ or $Mg_{(2b)}^{2+}$ positions in Table 5. It can be seen that at the parameterised model 3 (PM3) and HF/6-31G levels, the $Mg_{(2a)}^{2+}$ position clearly favours reaction by over

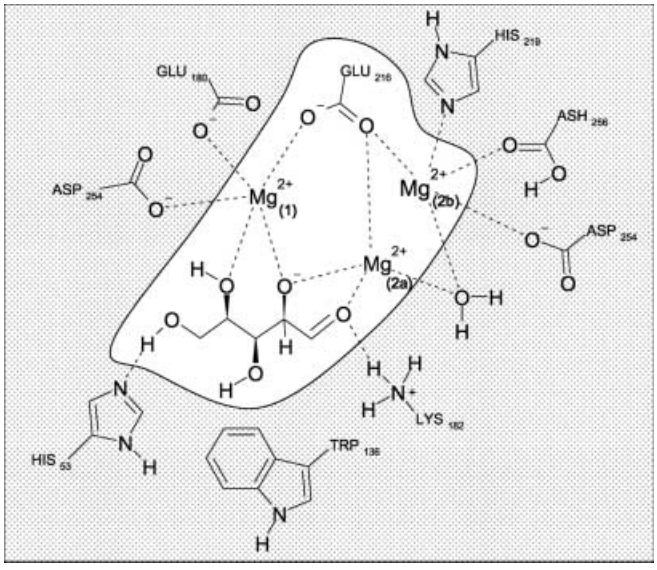

Fig. 6. The 12-residue and three-residue (*not shaded*) QM/MM active site models. The two alternative positions for $Mg_{(2)}^{2+}$ are shown as *(2a)* and *(2b)*

15 kcalmol^{-1} and will thus only be considered in further studies. Here the electrostatic interaction with the surrounding residues stabilises the positive charge on the magnesium ion.

Now moving on to the actual activation barriers we can see that the semiempirical and ab initio HF/6-31G methods give similar values of 35 and 40 kcalmol^{-1}, respectively, but higher-level density functional studies result in a considerable lowering of the barrier to 27 kcalmol^{-1}; however, this value is still somewhat higher than those estimated from experiment of between 14 and 18 kcalmol^{-1}.

A recurring problem of QM/MM methods is the choice of the QM region. Quite often the choice of the partitioning between QM and MM regions can affect the reaction energetics owing to an imbalance of polarisation or charge transfer effects on and by neighbouring groups. In order to quantify this effect for the small models previously described, we considered a larger QM region, including an additional eight residues and a water molecule, which we shall hence refer to as the large (12-residue) model consisting of 133 atoms (Fig. 6). This system, which was constructed from the alternative 4XIS crystal structure, was also studied with a small three-residue QM region analogous to that described earlier. The activation barriers for the hydride shift reaction are shown in Table 6 with all geometries optimised at the PM3 level. The barrier is lowered by 10 kcalmol^{-1} with the larger region at the PM3 level and by 17 kcalmol^{-1} using the three-parameter hybrid method of Becke with the Lee, Yang and Parr correlation functional (B3LYP/6-31G**), although the absolute values from the latter method may not be reliable since they are evaluated at the PM3 stationary points. The increased relative stabilisation of the transition state which can thus be achieved with an increase in the size of the QM region is estimated to be of the order of 10–18 kcalmol^{-1} which when applied to the 6XIM three-residue barrier previously optimised at the higher theoretical levels would bring them more in line with experimental predictions.

Table 5. Activation barriers (ΔE/kcalmol^{-1}) with the three-residue (6XIM) QM/MM model for the two alternative positions of $Mg_{(2)}{}^{2+}$, (2a) and (2b)

QM/MM method	ΔE with $Mg_{(2a)}{}^{2+}$	ΔE with $Mg_{(2b)}{}^{2+}$
PM3	34.9	60.0
HF/6-31G	39.7	55.3
B3LYP/6-31G	27.4	–
B3LYP/6-31G*	27.1	–

Table 6. Activation barriers (kcalmol^{-1}) with the small and large (4XIS) QM/MM models

QM method	Small (three-residue) model	Large (12-residue) model
PM3	42.1	24.9
B3LYP/6-31G**//PM3	15.0	4.8

Another important result from the larger QM region calculations is the shape of the potential-energy surface which will contribute to the KIEs. The optimised transition states were both fully characterised at the PM3 level and the single imaginary frequencies, 1291i and 1281i cm^{-1} with the small and large QM regions, respectively, are quite similar and we may have some confidence in KIEs studied with the smaller QM region.

3.4 Evaluation of KIEs

One of the most frequently used experimental approaches for the determination of enzyme reaction mechanism is the use of hydrogen/deuterium primary KIEs. Here, using the three-residue (6XIM) QM/MM model and the corresponding potential-energy surface, calculated as outlined in the previous section, we evaluated the rate constants for the hydride shift step using semiclassical VTST as implemented in the POLYRATE code [36]. These rate constants, which are based upon TST with quantised vibrational partition functions and semiclassical multidimensional tunnelling contributions, were computed from a QM/MM reaction path. The minimum energy path was found using the method of Page and McIver [37] in mass-scaled coordinates and was facilitated by our fixed link atom scheme since the terminating hydrogens can be assigned infinite masses throughout the optimisation steps and frequency evaluations.

The determination of rate constants using the canonical VTST (CVTST) method was accomplished firstly by location of the maximum in the free energy of activation and subsequent calculation of the rate constant by TST. The calculation of the free energies of activation along the path requires the appropriate vibrational partition function. However, the Hessians that are needed for this step render such VTST calculations computationally expensive, so we only present results calculated using the PM3 QM/MM potential-energy surface. Furthermore, to reduce the number of Hessians that are required we used the interpolated VTST by mapping method [38]. We sampled a limited potential-energy surface between -1.5 and $1.0a_0$ from the transition state and extrapolated to $\pm\ 2.0a_0$, where the tunnelling probability becomes insignificant (below 10^{-8}). This involved 250 Hessians and 500 gradient evaluations. We also computed the rate constants using conventional TST using the saddle point of the potential-energy surface. For this reaction we find that there is little difference between the TST and CVTST methods.

Finally the rate constants were corrected for QM motions in the reaction coordinate by using the microcanonical optimised multidimensional tunnelling approximation. Two models that consider either zero curvature tunnelling (ZCT) or small curvature tunnelling (SCT) paths [40, 41] were studied and are compared to the results using the simpler Wigner correction [39]. The primary KIEs for the hydride shift reaction calculated using these methods are summarised in Table 7.

Table 7. Primary H/D kinetic isotope effects (*KIEs*) for the three-residue (6XIM) QM/MM potential-energy surface using semiclassical variational transition state theory (*VTST*) at the PM3 level. The tunnelling correction method is given in *parentheses*

Temperature (K)	CVTST (no tunnelling)	TST (Wigner)	CVTST (zero curvature tunnelling)	CVTST (small curvature tunnelling)
298	2.4	3.0	4.8	6.3
323	2.3	2.8	3.9	4.7
333	2.2	2.7	3.6	4.3
348	2.1	2.6	3.3	3.8

Table 8. Primary H/D KIEs using the B3LYP/6-31G method and the three-residue (6XIM) PM3 QM/MM potential-energy surface (B3LYP/6-31G///PM3)

Temperature (K)	CVTST (no tunnelling)	TST (Wigner)	CVTST (zero curvature tunnelling)	CVTST (small curvature tunnelling)
298	3.4	4.0	5.2	5.8
323	3.1	3.6	4.4	4.7
333	3.0	3.4	4.1	4.4
348	2.8	3.3	3.8	4.1

Although these calculations are generally feasible for quite large systems using semiempirical Hamiltonians (PM3), they may be computationally prohibitive for even quite small systems when high levels of theory are employed. For this reason the so-called dual level approach is frequently used where information on the full pathway is computed at the lower PM3 level of theory and is scaled by more limited information from the transition state at the higher B3LYP/6-31G level [42, 43]. This method is used here and is denoted B3LYP/6-31G///PM3. The KIEs calculated using this approach are presented in Table 8.

We may now compare the resulting KIE values from the range of methods and investigate the importance of the tunnelling corrections. The origin of the discrepency between the calculated KIE data and the experimental prediction of 2.7 at 333 K [10] is unclear. Although TST with the simpler Wigner correction (1.2 at 333 K) is in agreement with experiment, the higher-level ZCT and SCT corrections are larger, between 1.6 and 2.0 at 333 K. These values are suggestive that either the theoretical level of the TST calculation or the potential-energy surface may not be accurate enough. However, with the higher-level B3LYP/6-31G///PM3 method the KIEs are even larger.

4 Conclusions

Clearly the study of the dynamics of hydrogen transfer, including tunnelling and protein motion, is a formidable problem. However we have demonstrated how QM/MM methods can be used with VTST and multidimensional tunnelling to study the KIEs of enzyme reactions. Although the effects have proven relatively small for xylose isomerase, the techniques may prove useful for other systems currently under study where more significant tunnelling is thought to occur. However, the ZCT and SCT corrections for xylose isomerase have been shown to be significantly larger than the simple Wigner correction.

We have shown that the choice of QM/MM model is important to balance transition-state stabilisation by neighbouring groups and that density functional theory methods are often necessary to determine accurate energetics. We have also shown that the link atom scheme commonly used for partitioning QM and MM regions across covalent bonds is quite reliable and that the LSCF scheme may offer little improvement unless optimised. For some simple model systems, we have demonstrated how two simple approaches involving auxiliary density basis functions or scaling of the charges can enhance the accuracy of the LSCF method towards that of a fully QM calculation.

Acknowledgements. We thank D.G. Truhlar for the use of his POLYRATE code, C.I.F. Watt for helpful discussions and EPSRC for financial support.

References

1. Watt CIF (1998) In: Sinnot M (ed) Comprehensive biological catalysis. Academic, New York, p 253
2. Allen KN, Lavie A, Farber GK, Glasfeld A, Petsco GA, Ringe D (1994) Biochemistry 15: 5627
3. Smith CA, Rangarajan M, Hartley BS (1991) Biochem J 277: 255
4. Jenkins J, Hanin J, Rey F, Chiadmi M, van Tilbeurgh H, Lasters I, De Maeyer M, van Belle D, Wodak SJ, Lauwereys M, Stanssens P, Mrabet NT, Snauwaert J, Matthyssens G, Lambeir AM (1992) Biochemistry 31: 5449
5. Lambeir AM, Lauwereys M, Stanssens P, Mrabet NT, Snauwaert J, Vantilbeurgh H, Matthyssens G, Lasters I, Demaeyer M, Wodak SJ, Jenkins J, Chiadmi M, Janin J (1992) Biochemistry 31: 5459
6. Whitlow M, Howard AJ, Finzel BC, Poulas TL, Winborne E, Gilliland GL (1991) Proteins 9: 153
7. van Bastelaere PBM, Kersters-Hilderson HLM, Lambeir AM (1995) Biochem J 307: 135
8. Zheng Y-J, Merz KM, Farber GK (1993) Protein Eng 6: 479
9. Fuxreiter M, Farkas O, Naray-Szabo G (1995) Protein Eng 8: 925
10. Hu H, Liu H, Shi Y (1997) Proteins 27: 545
11. Asboth B, Bocskei Z, Fuxreiter M, Naray-Szabo G (1997) In: Banci L, Comba P (eds) Molecular modeling and dynamics of bioinorganic systems. Kluwer, Dordrecht, p 419
12. Warshel A, Levitt M (1976) J Mol Biol 103: 227
13. Singh UC, Kollman PA (1986) J Comput Chem 7: 718
14. Field MJ, Bash PA, Karplus M (1990) J Comput Chem 11: 700
15. Gao J (1997) In: Lipkowitz KB, Boyd DB (eds) Reviews in computational chemistry, vol 7. VCH, New York, p 119
16. Truhlar DG, Garrett BC, Klippenstein SJ (1996) J Phys Chem 100: 12771
17. Alhambra C, Gao JL, Corchado JC, Villa J, Truhlar DG (1999) J Am Chem Soc 121: 2253
18. Hart JC, Hillier IH, Burton NA, Sheppard DW (1998) J Am Chem Soc 120: 13535
19. Harrison MJ, Burton NA, Hillier IH (1997) J Am Chem Soc 119: 12285
20. Burton NA, Harrison MJ, Hart JC, Hillier IH, Sheppard DW (1998) Faraday Discuss 110: 463

21. Cornell WD, Cieplak P, Bayly CI, Gould IR, Merz KM, Ferguson DM, Spellmeyer DC, Fox T, Caldwell JW, Kollman PA (1995) J Am Chem Soc 117: 5179
22. Assfeld X, Rivail J-L (1996) Chem Phys Lett 263: 100
23. Gao J, Amara P, Alhambra C, Field MJ (1998) J Phys Chem A 102: 4714
24. Antes I, Thiel W (1999) J Phys Chem A 103: 9290
25. Reuter N, Dejaegere A, Maigret B, Karplus B (2000) J Phys Chem A 104: 1720
26. Philipp DM, Friesner RA (1999) J Comput Chem 20: 1468
27. Zhang Y, Lee T-S, Yang W (1999) J Chem Phys 110: 46
28. Frisch MJ, Trucks GW, Schlegel HB, Gill PMW, Johnson BG, Robb MA, Cheeseman JR, Keith TA, Petersson GA, Montgomery JA, Raghavachari K, Al-Laham MA, Zakrzewski VG, Ortiz JV, Foresman JB, Cioslowski J, Stefanov BB, Nanayakkara A, Challacombe M, Peng CY, Ayala PY, Chen W, Wong MW, Andres JL, Replogle ES, Gomperts R, Martin RL, Fox DJ, Binkley JS, Defrees DJ, Baker J, Stewart JP, Head-Gordon M, Gonzales C, Pople JA (1995) GAUSSIAN94. Gaussian, Pittsburgh, Pa
29. Pearlman DA, Case DA, Caldwell JW, Ross WS, Cheatham TE, Ferguson DM, Seibel GL, Singh UC, Weiner PK, Kollman PA (1995) AMBER 4.1. University of California, San Francisco
30. Besler BH, Merz KM, Kollmann PA (1990) J Comput Chem 11: 431
31. Hall RJ, Hindle SA, Burton NA, Hillier IH (2000) J Comput Chem 21: 1433
32. Hindle SA (2000) PhD thesis. University of Manchester, Manchester, UK
33. Boys SF (1960) Rev Mod Phys 32: 296
34. Pipek J, Mezey PG (1989) J Chem Phys 90: 4916
35. Brooks BR (1998) CETEP workshop. Lyon, France
36. Steckler R, Chuang Y-Y, Fast PL, Coitiño EL, Corchado JC, Hu W-P, Liu Y-P, Lynch GC, Nguyen KA, Jackels CF, Gu MZ, Rossi I, Clayton S, Melissas VS, Garrett BC, Isaacson AD, Truhlar DG (1997) POLYRATE, version 7.4. University of Minnesota, Minneapolis
37. Page M, McIver JW (1988) J Phys Chem 88: 922
38. Corchado JC, Coitiño EL, Chuang YY, Fast PL, Truhlar DG (1998) J Phys Chem A 102: 2424
39. Bell RP (1980) The tunnel effect in chemistry. Chapman and Hall, London
40. Skodje RT, Truhlar DG, Garrett BC (1981) J Phys Chem 85: 3019
41. Liu Y-P, Lynch GC, Truong TN, Lu D-H, Truhlar DG, Garrett BC (1993) J Am Chem Soc 115: 2408
42. Corchado JC, Espinosa-Garcia J, Hu WP, Rossi I, Truhlar DG (1995) J Phys Chem 99: 687
43. Chuang YY, Truhlar DG (1997) J Phys Chem A 101: 3808; erratum (1997) J Phys Chem A 101: 8741